

INTRINSIC PROPERTIES OF THE MAGNETICALLY COLLIMATED H₂O MASER JET OF W43AW. H. T. VLEMMINGS¹, P. J. DIAMOND¹
Astrophysical Journal Letters accepted 07/14/06

ABSTRACT

Water maser polarization observations in the precessing jet of W43A have revealed that it is magnetically collimated. Here we present a detailed description of the physical properties of the water maser environment in the jet. We discuss the maser saturation level and beaming angle as well as the intrinsic temperatures and densities. Additionally, we show that the polarization angle of the strongest red-shifted maser feature undergoes a fast rotation of 90° across the maser. Along with the variation of linear polarization fraction, this strongly supports the current theoretical description of maser linear polarization.

Subject headings: Stars:individual (W43A)—magnetic fields—polarization—masers

1. INTRODUCTION

W43A is an evolved star at a distance of 2.6 kpc (Diamond et al. 1985) and is surrounded by a thick circumstellar envelope (CSE) that exhibits OH, H₂O and SiO masers (Imai et al. 2005, and references therein). Unlike the shell-like structure of the 22 GHz H₂O masers typically found in the envelopes of evolved stars, the H₂O masers of W43A occur in two clusters at 1000 AU from the star near the opposing tips of a collimated jet. The jet, with a velocity of 145 km s⁻¹, has an inclination of 39° with respect to the sky plane, a position angle of 65° and shows a 5° precession with a period of 55 years. The inferred dynamical age of the jet is only approximately 50 years (Imai et al. 2002). W43A is interpreted as belonging to a class of objects undergoing a rapid transition from an evolved star into a planetary nebula (PNe). Owing to their short expected lifetime of less than 1000 years, only 4 sources of this class have been identified to date (Imai et al. 2002, 2004; Likkel et al. 1992; Morris et al. 2003; Boboltz & Marvel 2005). H₂O masers at 22 GHz are excited in gas with temperatures of $T \approx 400$ K and hydrogen number densities of $n = 10^8 - 10^{10}$ cm⁻³ (Elitzur 1992). These conditions are typically found close to the star. The H₂O masers in the collimated jet of W43A, however, likely arise when the jet has swept up enough material previously expelled from the star so that conditions at the tip of the jet have become favorable for H₂O masers to occur. Alternatively, they occur in a shock between the collimated jet and dense material in the outer CSE, similar to the H₂O masers found in star-forming regions.

Observations of linear and circular polarization of the different maser species in CSEs are uniquely suited to study the strength and structure of magnetic fields. Close to the central star, at radii of 5–10 AU, SiO masers indicate ordered fields of the order of several Gauss (e.g. Kemball & Diamond 1997; Herpin et al. 2006). At the outer edge of the CSE, the polarization measurements of OH masers reveal milliGauss magnetic fields and indicate weak alignment with CSE structure (e.g Etoka & Diamond 2004). Recently, the Zeeman splitting giving rise to the circular polarization of H₂O masers was measured for a sample of evolved stars (Vlemmings et al. 2002, 2005). It was shown that at distances of several tens to hundreds

of AU, CSEs harbor large scale magnetic fields with typical field strengths between a few hundred milliGauss up to a few Gauss. While the origin of the magnetic field is still unclear, theoretical models have shown that a dynamo between the slowly rotating stellar outer layers and the faster rotating core can produce the observed magnetic fields (Blackman et al. 2001). However, this likely requires an additional source of angular momentum to maintain the magnetic field, which could be provided by the presence of a binary companion or heavy planet (Blackman 2004).

Magnetic fields around evolved stars are thought to be one of the main factors in shaping the CSEs and producing the asymmetries during evolution of a spherically symmetric star into the often asymmetric PN. Theoretical models show that magnetic fields could be the collimating agents of the bi-polar jets in young proto-planetary nebulae such as W43A (e.g García-Segura et al. 2005). In a recent paper, we have shown, using H₂O maser linear and circular polarization observations, that the magnetic field is indeed the collimating agent of the jet of W43A (Vlemmings et al. 2006, hereafter paper I). Here we present a more detailed analysis of the observations presented in paper I. We discuss the physical properties of the maser region. We also show how the observed linear polarization characteristics strongly support the current maser theory.

2. OBSERVATIONS

The observations of W43A were performed with the NRAO² VLBA on December 8 2004 at the frequency of the 6₁₆ – 5₂₃ rotational transition of H₂O: 22.235080 GHz. We used 4 baseband filters of 1 MHz width, which were pairwise overlapped to get a velocity coverage of ≈ 25 km s⁻¹ around both the blue-shifted ($V_{\text{lsr}} = -56$ km s⁻¹) and red-shifted ($V_{\text{lsr}} = 124$ km s⁻¹) tip of the H₂O maser jet. Similar to the observations of H₂O masers in star-forming regions described in Vlemmings et al. (2006, hereafter V06), the data were correlated multiple times with a correlator averaging time of 8 sec. The initial correlation was performed with modest spectral resolution (128 channels; 7.8 kHz = 0.1 km s⁻¹), which enabled us to generate all 4 polarization combinations (RR, LL, RL and LR). Two additional correlator runs were performed with high spec-

² The National Radio Astronomy Observatory (NRAO) is a facility of the National Science Foundation operated under cooperative agreement by Associated Universities, Inc.

¹ Jodrell Bank Observatory, University of Manchester, Macclesfield, Cheshire SK11 9DL, U.K.; wouter@jb.man.ac.uk

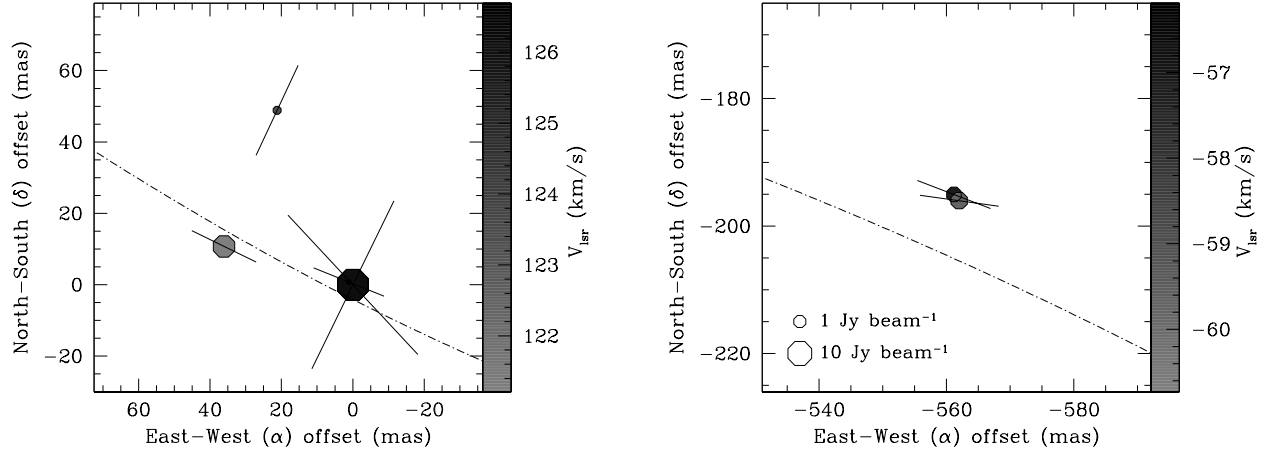


FIG. 1.— The H_2O maser features for which polarization was detected in the red- (left) and blue-shifted (right) tips of the jet of W43A. The symbols are scaled logarithmically according to peak flux and the grey-scale indicates their velocity. The linear polarization vectors are scaled logarithmically as a function of polarization percentage. The dashed-dotted line indicates the precessing jet model.

tral resolution (512 channels; $1.95 \text{ kHz} = 0.027 \text{ km s}^{-1}$), which therefore only contained the two polarization combinations RR and LL, to be able to detect the signature of the H_2O Zeeman splitting across the entire velocity range. The observations on W43A were interspersed with 15 minute observations of the polarization calibrator J1743-0350. Including scans on the phase calibrators (3C345 and 3C454.3), the total observation time was 8 hours. The data analysis path is described in detail in Vlemmings et al. (2002) and follows the method of Kemball et al. (1995). Fringe fitting and self-calibration were performed on a strong ($\sim 35 \text{ Jy beam}^{-1}$) maser feature (at $V_{\text{lsr}} = -15.72 \text{ km s}^{-1}$). Image cubes were created of Stokes I, Q and U from the intermediate spectral resolution data and of Stokes I and V with high spectral resolution. Due to the low declination of W43A ($\alpha(\text{J2000}) = 18h47m41.166s$ and $\delta(\text{J2000}) = -01^\circ 45' 11.7''$), the beam width is $\approx 0.6 \times 1.3 \text{ mas}$. In the high spectral resolution total intensity and circular polarization channel maps, the noise is $\approx 14 \text{ mJy beam}^{-1}$. In the lower spectral resolution Stokes Q and U maps the rms noise is $\approx 10 \text{ mJy beam}^{-1}$. We estimate our polarization angles to contain a possible systematic error of $\sim 8^\circ$ due to the error in the polarization angle of the calibrator J1743-0350.

3. RESULTS

We detected polarization in several 22 GHz H_2O maser features in both the red-shifted and blue-shifted tips of the jet of W43A. The complete map of detected maser features is shown in Figure 1 of paper I. Here we show, in Fig. 1, the maser features for which linear polarization was detected. In Table 1 we list the position off-sets with respect to the reference feature ($\Delta\alpha$ and $\Delta\delta$), peak flux, full-width half maximum line-width (Δv) and LSR velocity (V_{lsr}) of these maser features. The table also contains the fractional linear polarization (P_L), polarization angle (χ), fractional circular polarization (P_V) and magnetic field strength (B) determined at angle θ from the line-of-sight. The polarization properties and corresponding rms errors are determined from a flux weighted average over Δv for each maser line. We only detected circular polarization, at a level of 3.7σ , in one of the blue-shifted maser features (feature 5),

and its polarization spectrum is shown in Figure 2 of paper I. The magnetic field strength and 3σ field strength upper limits were determined as described in V06. This analysis resulted in an estimate of $B \cos\theta = 85 \pm 33 \text{ mG}$ for the feature where circular polarization was detected.

We have detected linear polarization in the six brightest maser features. As discussed in paper I, the weighted mean linear polarization fraction of these masers is $0.66 \pm 0.07\%$ and the 3σ upper limits in the masers where no linear polarization was detected range upwards from 0.68% . In the brightest of the maser features (feature 1), we observe a 90° flip of polarization angle across the maser, which is shown in Fig. 2. This is not observed for any of the other maser features. The fractional polarization of feature 1 also varies across the maser and the values in Table 1 represent the values at the location of the maximum and minimum polarization angle. The flux weighted average of the linear polarization fraction of the maser feature is $0.99 \pm 0.49\%$.

4. DISCUSSION

4.1. Intrinsic properties of the maser regions

As described in V06, the models used to determine the magnetic field from the maser total intensity and polarization spectra also yield the intrinsic maser thermal width $\Delta v_{\text{th}} \approx 0.5(T/100)^{1/2}$, where T is the temperature in the maser region. Additionally, the models produce the maser emerging brightness temperature $T_b \Delta\Omega$, where T_b is the brightness temperature and $\Delta\Omega$ the unknown beaming solid angle. Circular polarization measurements are necessary to optimally constrain Δv_{th} and $T_b \Delta\Omega$, and we have been able to determine Δv_{th} and $T_b \Delta\Omega$ for one of the maser features. We find that the intrinsic thermal width of feature 5, in the blue-shifted tip of the jet, is $\Delta v_{\text{th}} = 1.1 \pm 0.3 \text{ km s}^{-1}$. This indicates an intrinsic temperature in the maser jet of $T \approx 500 \text{ K}$. For the emerging brightness temperature we find $T_b \Delta\Omega \approx 8 \times 10^9 \text{ K sr}$.

The masers in the collimated jet of W43A are found at $\sim 1000 \text{ AU}$ from the central star, much further out than is typical for the H_2O masers in the CSE of evolved stars. They likely arise when the jet has swept up enough ma-

TABLE 1
W43A MASER FEATURES

feature	$\Delta\alpha$ (mas)	$\Delta\delta$ (mas)	peak intensity (Jy beam $^{-1}$)	Δv (km s $^{-1}$)	V_{lsr} (km s $^{-1}$)	P_L (%)	χ ($^{\circ}$)	P_V (%)	$B \cos \theta$ (mG)
1 ^a	0.0	0.0	38.57	0.54	126.11	2.29 ± 0.40	54 ± 3	-	< 36
						2.25 ± 0.42	-29 ± 1		
2	1.1	0.7	4.89	0.68	126.69	0.62 ± 0.23	68 ± 10	-	< 278
3	21.2	48.9	6.45	0.79	123.42	0.82 ± 0.23	-25 ± 12	-	< 306
4	36.1	10.7	18.66	0.75	121.21	0.59 ± 0.17	64 ± 4	-	< 101
5	-561.2	-195.0	10.85	0.88	-57.19	0.64 ± 0.19	69 ± 8	0.33 ± 0.09	85 ± 33
6	-562.0	-196.0	12.45	0.66	-59.73	0.65 ± 0.06	82 ± 6	-	< 93

NOTE.—^a polarization angle gradient across maser feature (see text)

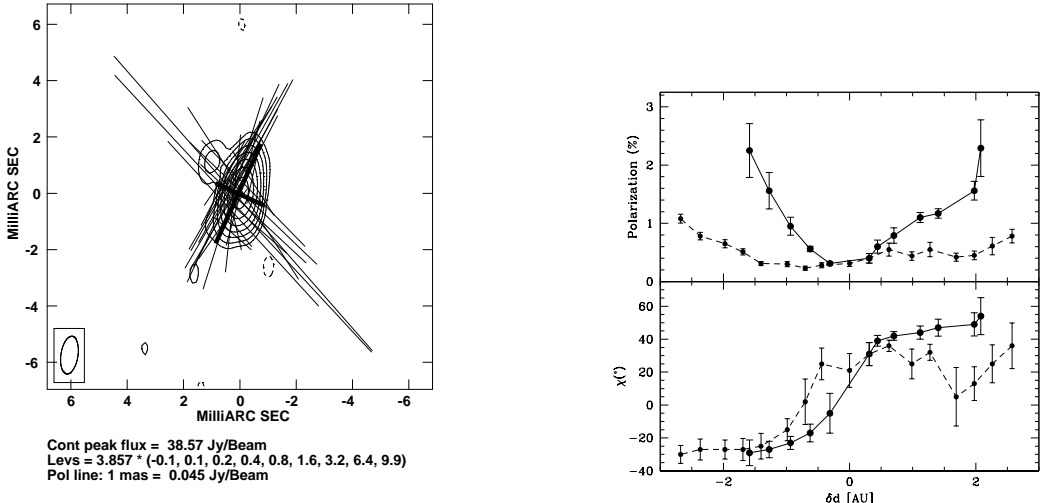


FIG. 2.— (left) Total intensity map of the strongest maser feature in the red-shifted tip of the jet of W43A at $V_{\text{lsr}} = 126.11$ km s $^{-1}$. The vectors indicate the linear polarization, the thick solid lines indicate the slices across the feature for which linear polarization angle and fractional linear polarization are shown at the right. (right) Fractional linear polarization (top) and polarization angle χ (bottom) versus angular offset for slices across the strongest maser feature. The offset δd is determined with respect to the position of the peak maser emission and assuming a distance to W43A of 2.6 kpc. δd increases towards the South. The thin dashed lines indicate the slice perpendicular to the jet direction at PA = -27° and the thick solid line indicates the slice along the jet direction at PA = 63° .

terial to create suitable conditions for maser excitation. Alternatively, the masers occur in a shocked region between the jet and dense material in the outer CSE, similar to the shocked masers found in star-forming regions. If the masers occur in a shock, the temperature in the maser region indicates that it is likely a dissociative J-shock (Kaufman & Neufeld 1996). Using the H₂O maser models developed for J-shock masers in star-forming regions (Elitzur et al. 1989), we then find that the pre-shock hydrogen density would be $n \sim 3 \times 10^6$ cm $^{-3}$. This is an order of magnitude higher than the typical hydrogen density at ~ 1000 AU from the star ($n \sim 10^5$ cm $^{-3}$). We thus conclude that the H₂O masers are likely excited in material swept up in the jet instead of in a J-shock.

We can compare the emerging brightness temperature determined from the model, with the maser brightness temperature determined from the observations. We find that feature 5 is unresolved. Assuming a size of ~ 0.4 mas,

which corresponds to ≈ 1 AU, we find a brightness temperature lower limit $T_b \gtrsim 1.5 \times 10^{11}$ K. Thus, the upper limit on the beaming solid angle $\Delta\Omega \lesssim 5 \times 10^{-2}$ sr, which is similar to the values found in star-forming regions (V06). Most of the other maser features are also unresolved, with only the brightest feature (feature 1) being marginally resolved. Thus, the W43A H₂O masers have brightness temperatures of $T_b \approx 10^{11} - 10^{12}$ K. Additionally, we can compare the emerging brightness temperature with the maser brightness temperature T_S at the onset of saturation. Using Reid & Moran (1988), we find $T_S \Delta\Omega = 3.4 \times 10^9$ K sr. This indicates, for $\Delta\Omega \approx 5 \times 10^{-2}$ sr, that the masers of W43A are mostly saturated.

4.2. Linear Polarization

Maser theory has shown that the percentage of linear polarization P_L of H₂O masers depends on the degree of saturation and the angle θ between the maser propagation

direction and the magnetic field (e.g. Deguchi & Watson 1990). Additionally, when the Zeeman frequency shift $g\Omega$ is much greater than the rate for stimulated emission R , the polarization vectors are either perpendicular or parallel to the magnetic field lines, depending on θ . For the typical emerging brightness temperature in the H₂O maser jet of W43A, $T\Delta\Omega \approx 10^{10}$ K sr, $R \approx 1$ s⁻¹, while for a magnetic field of ≈ 100 mG, the strongest 22 GHz hyperfine transitions have $g\Omega \sim 1000$ s⁻¹. Thus $g\Omega \gg R$ is easily satisfied. As a result, when $\theta > \theta_{\text{crit}} \approx 55^\circ$ the polarization vectors are perpendicular to the magnetic field, and when $\theta < \theta_{\text{crit}}$ they are parallel (Goldreich et al. 1973). The strongest linear polarization is found when $\theta > \theta_{\text{crit}}$, thus it was concluded in paper I that most of the linear polarization vectors were perpendicular to the magnetic field, indicating a toroidal magnetic field configuration. If alternatively they are parallel to the magnetic field we are actually probing the poloidal component.

When θ is close to θ_{crit} , the linear polarization vectors can flip 90° on very small scales. According to maser theory, a minimum in P_L occurs when $\theta = \theta_{\text{crit}}$. This can be seen in figure A.1 of V06, which gives P_L as a function of θ and saturation level. Here, we observe a 90° flip across the brightest of the maser features in the jet of W43A, as shown in Fig. 2. Similar flips were observed in circumstellar SiO masers (Kemball & Diamond 1997) and H₂O masers in star-forming regions (V06). However, here we have for the first time been able to detect the expected minimum in P_L when the flip occurs. The minimum is most pronounced in the slice across the maser along the PA of the jet. The linear polarization characteristics are dominated by the condition along the maser path where the strongest amplification occurs (Vlemmings 2006). Thus, we conclude that the strongest amplification in the maser region giving rise to feature 1 occurs at the location along the line-of-sight where θ is close to θ_{crit} . The position angle changes from $\chi = 54^\circ$, which is perpendicular to the magnetic field, to $\chi = -29^\circ$, which is parallel to the magnetic field. Most of the other maser features have polarization angles that are perpendicular to the magnetic field except possibly feature 3 with $\chi = -25^\circ$, possibly because this maser feature is located at the edge of the jet, where a projected toroidal magnetic field will lie along the jet.

4.3. Magnetic Field

After correcting for the angle between the line-of-sight and the magnetic field, and taking into account the saturation level, we find a toroidal magnetic field of $B \approx 200$ mG in the H₂O maser jet of W43A (paper I). The magnetic field is increased in the density-enhanced H₂O maser jet due to partial coupling to the gas. The magnetic field outside the jet is found to be $B \approx 0.9 - 2.6$ mG if the masers exist in swept up material at a density of $n = 10^8 - 10^{10}$ cm⁻³. If the masers are excited in a dissociative shock, the magnetic field outside the jet is $B \approx 0.07$ mG, however, as discussed above, this is unlikely to be the case. In paper I it was shown that if we are probing the toroidal field, with $B_\phi \propto r^{-1}$, this implies an average magnetic field of $B \approx 20$ G on the surface of the star. This is in excellent agreement with the magnetic field values determined by extrapolating the field strengths found using SiO, H₂O and OH maser observa-

tions throughout the CSEs of a large number of evolved stars. If, instead of the toroidal field, we are probing the poloidal field (with its radial component $B_r \propto r^{-2}$), the surface magnetic field would be a factor of $\sim 10^3$ larger. As this is inconsistent with the other observations, we conclude that the H₂O maser polarization vectors are indeed tracing the toroidal magnetic field.

5. CONCLUSIONS

Using polarization observations of the H₂O masers in the tips of the jet of W43A we have shown that the masers most likely occur in swept up material, and are not shock excited. The masers are saturated with a typical beaming solid angle of $\Delta\Omega \approx 5 \times 10^{-2}$ sr and occur at temperatures of $T \approx 500$ K. The polarization vectors trace the toroidal magnetic field, which has a density enhanced field strength of $B \approx 200$ mG. This implies, as shown in paper I, a magnetic field strength that is sufficiently strong to produce a magnetically collimated jet. Additionally, a 90° flip of the polarization angle and a corresponding minimum in fractional linear polarization is observed across the brightest maser feature. This strongly supports the current maser polarization theory.

This research was supported by a Marie Curie Intra-European fellowship within the 6th European Community Framework Program under contract number MEIF-CT-2005-010393.

REFERENCES

- Blackman, E. G. 2004, in ASP Conf. Ser. 313: Asymmetrical Planetary Nebulae III, ed. M. Meixner et al. (San Francisco: ASP), 401
- Blackman, E. G., Frank, A., Markiel, J. A., Thomas, J. H., & Van Horn, H. M. 2001, Nature, 409, 485
- Boboltz, D. A. & Marvel, K. B. 2005, ApJ, 627, L45
- Deguchi, S. & Watson, W. D. 1990, ApJ, 354, 649
- Diamond, P. J., Norris, R. P., Rowland, P. R., Booth, R. S., & Nyman, L.-A. 1985, MNRAS, 212, 1
- Elitzur, M. 1992, Astronomical masers (Dordrecht: Kluwer)
- Elitzur, M., Hollenbach, D. J., & McKee, C. F. 1989, ApJ, 346, 983
- Etoka, S. & Diamond, P. 2004, MNRAS, 348, 34
- García-Segura, G., López, J. A., & Franco, J. 2005, ApJ, 618, 919
- Goldreich, P., Keeley, D. A., & Kwan, J. Y. 1973, ApJ, 179, 111
- Herpin, F., Baudry, A., Thum, C., Morris, D., & Wiesemeyer, H. 2006, A&A, 450, 667
- Imai, H., Morris, M., Sahai, R., Hachisuka, K., & Azzollini F., J. R. 2004, A&A, 420, 265
- Imai, H., Nakashima, J.-i., Diamond, P. J., Miyazaki, A., & Deguchi, S. 2005, ApJ, 622, L125
- Imai, H., Obara, K., Diamond, P. J., Omodaka, T., & Sasao, T. 2002, Nature, 417, 829
- Kaufman, M. J. & Neufeld, D. A. 1996, ApJ, 456, 250
- Kemball, A. J. & Diamond, P. J. 1997, ApJ, 481, L111
- Kemball, A. J., Diamond, P. J., & Cotton, W. D. 1995, A&AS, 110, 383
- Likkel, L., Morris, M., & Maddalena, R. J. 1992, A&A, 256, 581
- Morris, M. R., Sahai, R., & Claussen, M. 2003, in Revista Mexicana de Astronomia y Astrofisica Conference Series, 20–22
- Reid, M. J. & Moran, J. M. 1988, Astronomical masers (Galactic and Extragalactic Radio Astronomy), 255–294
- Vlemmings, W. H. T. 2006, A&A, 445, 1031
- Vlemmings, W. H. T., Diamond, P. J., & Imai, H. 2006, Nature, 440, 58 (paper I)
- Vlemmings, W. H. T., Diamond, P. J., & van Langevelde, H. J. 2002, A&A, 394, 589
- Vlemmings, W. H. T., Diamond, P. J., van Langevelde, H. J., & Torrelles, J. M. 2006, A&A, 448, 597 (V06)
- Vlemmings, W. H. T., van Langevelde, H. J., & Diamond, P. J. 2005, A&A, 434, 1029